Draft version May 19, 2014
Preprint typeset using LaTeX style emulateapj v. 5/2/11

arXiv:1405.3986v1 [astro-ph.GA] 15 May 2014

DISCOVERY OF EIGHT $Z \sim 6$ QUASARS FROM PAN-STARRS1

E. Bañados [1], B.P. Venemans [1], E. Morganson [1], R. Decarli [1], F. Walter [1], K.C. Chambers [2], H-W. Rix [1], E.P. Farina[1], X. Fan[3], L. Jiang[4], I. McGreer [3], G. De Rosa[5], R. Simcoe[6], A. Weiss[7], P. A. Price[8], J. S. Morgan[2], W. S. Burgett[2], J. Greiner[9] , N. Kaiser[2], R.-P. Kudritzki[2], E. A. Magnier[2], N. Metcalfe[10], C. W. Stubbs[11], W. Sweeney [2], J. L. Tonry[2], R. J. Wainscoat[2], and C. Waters[2]

Draft version May 19, 2014

ABSTRACT

High-redshift quasars are currently the only probes of the growth of supermassive black holes and potential tracers of structure evolution at early cosmic time. Here we present our candidate selection criteria from the Panoramic Survey Telescope & Rapid Response System 1 and follow-up strategy to discover quasars in the redshift range $5.7 \lesssim z \lesssim 6.2$. With this strategy we discovered eight new $5.7 \leq z \leq 6.0$ quasars, increasing the number of known quasars at $z > 5.7$ by more than 10 %. We additionally recovered 18 previously known quasars. The eight quasars presented here span a large range of luminosities ($-27.3 \leq M_{1450} \leq -25.4$; $19.6 \leq z_{\rm P1} \leq 21.2$) and are remarkably heterogeneous in their spectral features: half of them show bright emission lines whereas the other half show a weak or no Lyα emission line (25% with rest-frame equivalent width of the Lyα+N v line lower than 15Å). We find a larger fraction of weak-line emission quasars than in lower redshift studies. This may imply that the weak-line quasar population at the highest redshifts could be more abundant than previously thought. However, larger samples of quasars are needed to increase the statistical significance of this finding.

Subject headings: cosmology: observations – quasars: emission lines – quasars: general – surveys: Pan-STARRS1

1. INTRODUCTION

High-redshift quasars provide us with unique information about the evolution of supermassive black holes (SMBHs), their host galaxies, and the intergalactic medium (IGM) at early cosmic time. Over the last decade, numerous studies have established a sample of roughly 60 quasars at $5.5 < z < 7.1$, mostly discovered using optical surveys such as the Sloan Digital Sky Survey (SDSS; Fan et al. 2001, 2003, 2004, 2006b) and the Canada-France High-z Quasar Survey (CFHQS; Willott et al. 2005, 2007, 2009, 2010b,a). Among the key results from these studies are the existence of SMBHs less than a gigayear after the big bang (e.g., Willott et al. 2003; Mortlock et al. 2011; De Rosa et al. 2013), and the presence of near complete Gunn–Peterson absorption, indicating a rapid increase in the IGM neutral fraction and the end of reionization at $z \sim 6$ (Fan et al. 2006a). These findings strongly suggest that fundamental changes are happening in the IGM at $6 \lesssim z \lesssim 7$. In addition, the initial formation and growth of these SMBHs is, however, not fully understood. In order to further study this important era in the history of the universe and better constrain the formation and evolution of early structures and SMBH, the discovery and characterization of a significant sample of quasars in this redshift range is crucial.

The Panoramic Survey Telescope & Rapid Response System 1 (Pan-STARRS1, PS1; Kaiser et al. 2002, 2010) 3π is surveying all the sky above declination $-30°$ in the filters $g_{\rm P1}$, $r_{\rm P1}$, $i_{\rm P1}$, $z_{\rm P1}$, and $y_{\rm P1}$ (Stubbs et al. 2010; Tonry et al. 2012). The PS1 3π survey maps yearly each region of the sky in two sets of pairs per filter. Each pair is taken during the same night. The second pair for $g_{\rm P1}$, $r_{\rm P1}$, and $i_{\rm P1}$ are obtained during the same lunation, whereas for $z_{\rm P1}$ and $y_{\rm P1}$ are observed approximately 5–6 months later. There are some regions of the sky that are not covered or have less coverage (i.e., 0 or 2 exposures per year) than the average survey mostly due to weather restrictions (especially for $g_{\rm P1}$, $r_{\rm P1}$, and $i_{\rm P1}$ bands because their observation pairs are taken within the same month) or areas falling into the camera chip gaps.

PS1 presents an excellent opportunity to perform high-redshift quasar searches for three reasons: (1) it covers a larger area than previous high-redshift quasar surveys, especially in the southern hemisphere; (2) it goes significantly deeper than SDSS in the reddest bands where $z \sim 6$ quasars are visible (current 5σ median limiting magnitudes are $g_{\rm P1} = 22.9$, $r_{\rm P1} = 22.8$, $i_{\rm P1} = 22.6$, $z_{\rm P1} = 21.9$, $y_{\rm P1} = 20.9$); and (3) the additional y-band ($\lambda_{\rm eff} = 9620$ Å; FWHM= 890 Å; Tonry et al. 2012) en-

banados@mpia.de
[1] Max Planck Institut für Astronomie, Königstuhl 17, D-69117, Heidelberg, Germany
[2] Institute for Astronomy, University of Hawaii, 2680 Woodlawn Drive, Honolulu, HI 96822, USA
[3] Steward Observatory, The University of Arizona, 933 North Cherry Avenue, Tucson, AZ 85721–0065, USA
[4] School of Earth and Space Exploration, Arizona State University, Tempe, AZ 85287, USA
[5] Department of Astronomy, The Ohio State University, 140 West 18th Avenue, Columbus, OH 43210, USA
[6] MIT-Kavli Center for Astrophysics and Space Research, 77 Massachusetts Avenue, Cambridge, MA, 02139, USA
[7] Max-Planck-Institut für Radioastronomie, Auf dem Hügel 69 D-53121 Bonn, Germany
[8] Department of Astrophysical Sciences, Princeton University, Princeton, NJ 08544, USA
[9] Max-Planck-Institut für extraterrestrische Physik, Giessenbachstrasse 1, 85748 Garching, Germany
[10] Department of Physics, Durham University, South Road, Durham DH1 3LE, UK
[11] Department of Physics, Harvard University, Cambridge, MA 02138, USA

ables the search for luminous quasars beyond the SDSS limit, $z > 6.5$. In early 2013, PS1 produced its first internal release of the 3π stacked catalog (PV1), which is based on the co-added PS1 exposures (see Metcalfe et al. 2013). This is the catalog used for the present work and it includes data obtained primarily during the period 2010 May–2013 March.

In Morganson et al. (2012), we presented our preliminary selection method for our quasar search when the stacked catalog was not available and reported the discovery of the first PS1 high-redshift quasar (PSO J215.1514–16.0417 [12] at $z = 5.73$). In this paper, we refined our selection criteria and made use of the deeper and more complete information in the new PS1 stacked catalog. Our aim was to discover quasars at $z \sim 6$ while minimizing the contamination of foreground objects. This was possible by focusing the search on the redshift range $5.7 \lesssim z \lesssim 6.2$ where quasars and stars are best differentiated in PS1 colors (for details see Section 2). In this work we present our strategy and the first discoveries of this search.

The paper is organized as follows. In Section 2, we present our color selection procedures for $5.7 \lesssim z \lesssim 6.2$ quasars, including the initial selection from the PS1 stacked catalog and the follow-up optical and near-infrared (NIR) photometry. In Section 3, we present the discovery of eight new $z \sim 6$ quasars and discuss their spectral properties. In Section 4, we estimate our completeness by studying whether other quasars from the literature were or were not part of our list of candidates. We discuss how typical the weak-line emission quasars discovered in this work are in Section 5 and summarize our results in Section 6. Magnitudes throughout the paper are given in the AB system, except when referring to Two Micron All Sky Survey (2MASS) and Wide-field Infrared Survey Explorer (*WISE*) magnitudes which are in the Vega system, unless otherwise stated. We employ a cosmology with $H_0 = 69.3\,\mathrm{km\ s^{-1}\ Mpc^{-1}}$, $\Omega_M = 0.29$, and $\Omega_\Lambda = 0.71$ (Hinshaw et al. 2013).

2. SELECTION OF QUASAR CANDIDATES

Quasars at redshift $z \gtrsim 5.7$ are observationally characterized by their very red $i - z$ color and blue continuum (i.e., blue $z - y$ color). They are very faint or completely undetected in the i band due to the optically thick Lyα forest at these redshifts, causing most of the light coming from wavelengths $\lambda_{\rm rest} < 1216$ Å to be absorbed.

To determine the optimum selection criteria, we have taken the composite quasar spectrum from Decarli et al. (2010), which consists of 96 bright quasars at $0 < z < 3$. We chose this template because at red wavelengths it is less affected by host galaxy contamination than other composite spectra in the literature (e.g., Francis et al. 1991; Vanden Berk et al. 2001) and it samples the rest frame wavelengths of $5.7 < z < 7.2$ quasars in the PS1 filters. For $\lambda_{\rm rest} < 1010$ Å we replaced the template with a flat f_λ, normalized to the UV continuum blueward of Lyα. Then, we applied the intergalactic attenuation correction from Meiksin (2006), tuning the optical depth, $\tau_{\rm IGM}$, to match the transmitted flux blueward of Lyα in the $z \sim 6$ SDSS composite spectrum from Fan et al. (2006b). Figure 1 shows the expected track of our quasar template through the $i_{\rm P1} - z_{\rm P1}$ and $z_{\rm P1} - y_{\rm P1}$ colors as the redshift is increased from $z = 5.0$ to $z = 6.5$. We are also interested in the location of our potential contaminants in this diagram. Since the observational color scatter for brown dwarfs is significant, we decided to compare with real PS1 colors of known brown dwarfs. We cross-matched the ultracool dwarfs presented in Dupuy & Liu (2012) with the PS1 stacked catalog, taking the closest match within a $5''$ radius with proper motion measurements taken into account. There were 126 matches that had measurements in the $i_{\rm P1}$, $z_{\rm P1}$, and $y_{\rm P1}$ bands, and with a signal-to-noise ratio (S/N) > 10 in the $z_{\rm P1}$ band and S/N > 5 in the $y_{\rm P1}$ band. Their PS1 colors are represented by stars in Figure 1.

In this work we focused on the upper-left region of the color–color diagram in the right panel of Figure 1 for two reasons: (1) the bulk of the $z \sim 6$ quasar population is located there and (2) this is the region with the least brown dwarf contamination in this color–color diagnostic.

Because high-redshift quasars are very rare and because of the high number of other sources (or artifacts) that mimic high-redshift quasar colors, we cleaned our sample in several steps:

1. We selected initial high-redshift quasar candidates from the PV1 PS1 stacked database (see Section 2.1).
2. At the position of each candidate, we applied forced aperture photometry in the stacked images in order to corroborate the catalog colors (see Section 2.2).
3. This was followed by forced photometry in all single-epoch z-band images to remove artifacts (see Section 2.3).
4. We then matched the candidate list to the 2MASS (Skrutskie et al. 2006), SDSS DR8 (Aihara et al. 2011), and the UKIRT Infrared Deep Sky Survey (UKIDSS; Lawrence et al. 2007) to eliminate contaminants that are evident when using the extra information provided by these surveys (see Section 2.4).
5. We then cross-matched the remaining candidates with known quasars (see Section 2.5) and visually inspected the stacked and single-epoch stamps to ensure that they are real.
6. We then obtained optical and NIR follow-up photometry (see Section 2.6).
7. Finally, we obtained spectra to confirm the nature and redshifts of the remaining candidates (see Section 2.7).

2.1. *Selection from Pan-STARRS1 Catalog*

We excluded the Galactic plane ($|b| < 20°$), and M31 ($7° <$ R.A.$< 14°$; $37° <$ Decl.$< 43°$) from our search. The catalog used in this work had no data between $92° <$ R.A.$< 132°$. After removing these regions, the effective area of our survey is $\sim 20,000$ square degrees or $\sim 1.9\,\pi$ steradian.

[12] We have slightly modified the name published in Morganson et al. (2012) from PSO J215.1512–16.0417 to PSO J215.1514–16.0417 based on the stacked catalog coordinates.

For our candidates, we required coverage in at least the three redder bands ($i_{\rm P1}$, $z_{\rm P1}$, and $y_{\rm P1}$) and that more than 85% of the expected point-spread function (PSF)-weighted flux in these bands was located in valid pixels (i.e., that the PS1 catalog entry has `PSF_QF` > 0.85). In order to estimate the fraction of objects missed by requiring coverage in these three bands and/or by being located in bad pixels, we cross-matched the PS1 catalog to sources in 2MASS with S/N > 10 and fainter than 14th magnitude in all the 2MASS bands. The magnitude cut is intended to avoid objects that would be saturated in the PS1 catalog. After applying the same coverage and pixel criteria we estimate that the percentage of missed objects is $\sim 7\%$. We also excluded those measurements for which the Image Processing Pipeline (Magnier 2006, 2007) flagged the result as suspicious (see Table 6 in Appendix A for details).

We limited our survey to candidates with $z_{\rm P1} > 18.0$, S/N > 10 in the $z_{\rm P1}$ band, and S/N > 5 in the $y_{\rm P1}$ band (Equations (1a), (1b), and (1c)). We treated objects that were or not detected in the $i_{\rm P1}$ band differently as summarized in Equation (1d). For the former we required a color $i_{\rm P1} - z_{\rm P1} > 2.2$, for the latter we were less conservative and required $i_{\rm P1,lim} - z_{\rm P1} > 2.0$, where $i_{\rm P1,lim}$ is the 3σ-limiting magnitude. One of our main contaminants are cool stars, which have similar $i - z$ colors to those of $z \gtrsim 5.7$ quasars but are redder in $z - y$. However, for quasars at $z \gtrsim 6.2$, a significant amount of flux in the z-band is also absorbed, making these objects redder in the $z - y$ color (see Figure 1). In this paper we aim to get the bulk of the $z \sim 6$ quasar population while at the same time reducing the contamination by L- and T-dwarfs. We produce a relatively pure sample by setting an upper limit in the $z_{\rm P1} - y_{\rm P1}$ color of 0.5 (see Equation (1e) and Figure 1). This constraint has the drawback of preventing us from finding typical quasars at $z \gtrsim 6.2$. Once we have a better understanding of our contaminants, we will relax this constraint to search for quasars at higher redshifts. In order to prevent contamination from low redshift interlopers we also put constraints in the $r_{\rm P1}$ and $g_{\rm P1}$ bands. In Equation (1f), we will require that either the object was detected with a S/N< 3 in the $r_{\rm P1}$ band, or that the flux in the band was negative (i.e., the object was not detected or there was no coverage), or that there was a break in color of $r_{\rm P1} - z_{\rm P1} > 2.2$. We required a non-detection or no coverage in the $g_{\rm P1}$ band (Equation (1g)), since we expect virtually null flux in this band from a $z \sim 6$ quasar. Quasars at these redshifts are expected to be unresolved. In an attempt to select point-like sources we require the aperture magnitudes and PSF magnitudes of our candidates to be consistent with each other within 0.3 mag at least in one of the detection bands ($z_{\rm P1}$ or $y_{\rm P1}$, see Equation (1h)).

We can summarize the catalog selection criteria as follows:

$$z_{\rm P1} > 18.0 \quad (1a)$$
$$\mathrm{S/N}(z_{\rm P1}) > 10 \quad (1b)$$
$$\mathrm{S/N}(y_{\rm P1}) > 5 \quad (1c)$$
$$((i_{\rm P1} < i_{\rm P1,lim}) \,\mathrm{AND}\, (i_{\rm P1} - z_{\rm P1} > 2.2)) \,\mathrm{OR}$$
$$((i_{\rm P1} > i_{\rm P1,lim}) \,\mathrm{AND}\, (i_{\rm P1,lim} - z_{\rm P1} > 2.0)) \quad (1d)$$
$$z_{\rm P1} - y_{\rm P1} < 0.5 \quad (1e)$$
$$(\mathrm{S/N}(r_{\rm P1}) < 3) \,\mathrm{OR}\, (\mathrm{flux}(r_{\rm P1}) \leq 0) \,\mathrm{OR}$$
$$(r_{\rm P1} - z_{\rm P1} > 2.2) \quad (1f)$$
$$(\mathrm{S/N}(g_{\rm P1}) < 3) \,\mathrm{OR}\, (\mathrm{flux}(g_{\rm P1}) \leq 0) \quad (1g)$$
$$(-0.3 < z_{\rm P1-aper} - z_{\rm P1} < 0.3) \,\mathrm{OR}$$
$$(-0.3 < y_{\rm P1-aper} - y_{\rm P1} < 0.3) \quad (1h)$$

2.2. *Forced Photometry on Stacked Images*

In order to confirm and check the PS1 catalog colors, we implemented an algorithm to compute aperture photometry on the stacked images. This algorithm retrieves $5' \times 5'$ stacked postage stamps images centered on the candidates and their respective stacked catalogs. Then, we computed the aperture that maximizes the S/N of bright stars in the field and used it to get the aperture photometry of the respective candidate in the image. Since the aperture photometry is noisier than the PSF photometry, we relaxed the color criteria and required Equations (1a), (1d), (1e), and (1f) to be consistent within 2σ with our own measurements from the stacked images. This step mainly got rid of candidates that had bad $i_{\rm P1}$ photometry in the catalog. This is not surprising since our candidates were very faint or not detected in the $i_{\rm P1}$ band, and large photometric errors are expected.

We found empirically that when the diameter of our computed optimal apertures (aperture_diameter) were smaller than $0''.75$ or greater than $3''.75$, the images had evident problems mostly related to background subtraction, causing unreliable catalog magnitudes. Thus, we only considered candidates with $0''.75 <$ aperture_diameter$(izy) < 3''.75$.

2.3. *Single Epoch Forced Photometry*

It is possible that a fraction of our candidates were moving objects, spurious objects, or artifacts that appeared as very bright sources in some of the individual exposures and did not appear in others. After stacking the images, such objects could still look like reasonable quasar candidates. For this reason, we performed forced aperture photometry on all *individual* single epoch z band images (the detection band with the highest S/N) by using the optimal aperture determined in Section 2.2. We flagged the images in which the S/N at the position of the candidate was S/N < 3 while, based on the magnitude of the candidate measured on the stacked image, a S/N > 5 was expected. We retained candidates that had less than 40% flagged images and that the standard deviation of the single epoch magnitudes was less than 1 mag. These criteria were determined based on tests performed with known quasars and objects that had a counterpart in SDSS and in the *WISE* (Wright et al. 2010).

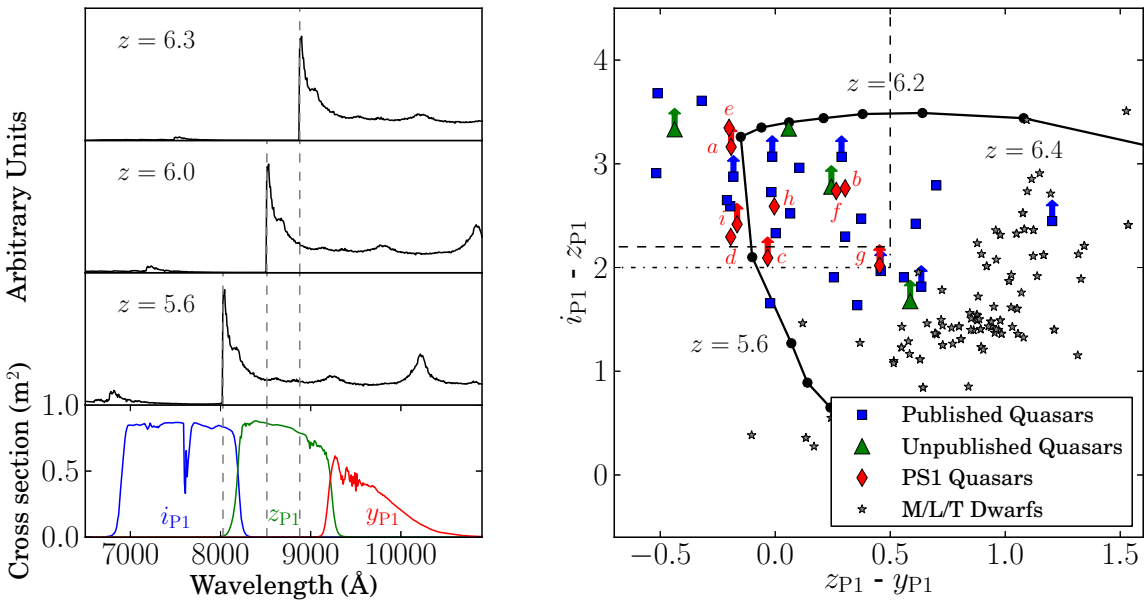

Figure 1. Left: the bottom panel shows the PS1 capture cross section in units of m^2 e^{-1} $photon^{-1}$ for the i_{P1}, z_{P1}, and y_{P1} bands (Tonry et al. 2012). The three upper panels show the composite quasar spectrum from Decarli et al. (2010) (with the intergalactic medium correction from Meiksin 2006) redshifted to $z = 5.6$, $z = 6.0$, and $z = 6.3$, from bottom to top. The gray dashed lines show the wavelength of the Lyα line at each redshift. Right: color–color diagram showing the criteria used to select quasar candidates (long-dashed line, upper left corner). The dot-dashed line is used for candidates with upper limits in the i_{P1} band. The thick black line shows the expected color of the quasar template from Decarli et al. (2010) redshifted from $z = 5.0$ to $z = 6.5$ in steps of $\Delta z = 0.1$ (see left panel). The M/L/T dwarfs from Dupuy & Liu (2012) that have a PS1 counterpart are shown with stars. Blue squares are published quasars at $5.7 < z < 6.4$ satisfying our S/N and coverage criteria. Fourteen of them were included in our candidate list. Green triangles represent the PS1 colors of unpublished spectroscopically confirmed $z \sim 6$ quasars (S.J. Warren et al., in preparation). Three of them were part of our candidate list (see Tables 4 and 5). The red diamonds are the new quasars presented in this paper (see Table 2). They are labeled with the following letters: a = PSO J340.2041–18.6621 ($z = 6.00$), b = PSO J007.0273+04.9571 ($z = 5.99$), c = PSO J037.9706–28.8389 ($z = 5.99$), d = PSO J187.3050+04.3243 ($z = 5.89$), e = PSO J213.3629–22.5617 ($z = 5.88$), f = PSO J183.2991–12.7676 ($z = 5.86$), g = PSO J210.8722–12.0094 ($z = 5.84$), h = PSO J215.1514–16.0417 ($z = 5.73$), and i = PSO J045.1840–22.5408 ($z = 5.70$).

2.4. *Cross-match with other Surveys*

We required our candidates to be either undetected in 2MASS or, similarly to Fan et al. (2001), that $z_{P1} - J_{2M} < 1.5$. We did forced photometry in the SDSS i-band (i_{SDSS}) and UKIDSS J-band (J_{UKIDSS}) when our candidates were in the area covered by these surveys. Candidates with S/N < 5 or that had S/N > 5 in the i_{SDSS} band and that satisfy $i_{SDSS} - z_{P1} > 2.0$ within 2σ errors were kept. We also retained objects that had $y_{P1} - J_{UKIDSS} < 1.5$.

2.5. *Cross-match with Known Quasars*

In order to avoid duplication with published quasars and other ongoing quasar search efforts, we removed fifteen published (including PSO J215.1514–16.0417) and three unpublished quasars (ULASJ1207+0630 at $z = 6.04$, ULASJ0148+0600 at $z = 5.96$, and ULASJ1243+2529 at $z = 5.83$; S.J. Warren et al., in preparation, but see also Mortlock et al. 2012) that were part of our candidate list. These quasars are discussed further in Section 4. All the remaining candidates were visually inspected.

2.6. *Imaging Follow-up*

Obtaining deeper optical and NIR photometry is essential to confirm the reality and colors of our candidates and to remove cool dwarfs with similar optical colors to quasars or contaminants that could have scattered into our color selection. The photometric follow-up observations were carried out over different observing runs and different instruments. We used GROND (Greiner et al. 2008), a $grizJHK$ simultaneous imager at the 2.2 m telescope in La Silla during 2012 May (when a small region of the stacked catalog was available) and 2013 January, typical on-source exposure times were 1440 s in the NIR and 1380 s in the optical. The ESO Faint Object Spectrograph and Camera 2 (EFOSC2; Buzzoni et al. 1984) at the ESO New Technology Telescope (NTT) was used to perform imaging in the $i\#705$ (I_{EFOSC2}) and $z\#623$ (Z_{EFOSC2}) bands during 2013 March with on-source exposure times of 300 s. We used the Omega2000 camera (Bizenberger et al. 1998) at the 3.5m telescope in Calar Alto to perform imaging with the z (z_{O2000}), Y (Y_{O2000}), and J (J_{O2000}) filters during 2013 March–June with 300 s exposure time on-source. The data reduction was carried out using standard reduction steps, consisting of bias subtraction, flat fielding, sky subtraction, image alignment, and finally stacking. The photometric zero points of the stacked images were calculated by using at least 5 stellar sources ($|mag_{P1-aper} - mag_{P1}| < 0.2$) in the images with magnitudes and colors from the PV1 catalog. Since all the filter curves are not exactly the same, conversions between PS1 and GROND/EFOSC2/Omega2000 magnitudes were computed as follows: first, we computed spectral synthetic magnitudes of template stars of various spectral classes (O – K) in each photometric system. We then produced color–color diagrams for various filters (e.g., $i_{GROND} - i_{P1}$ vs $i_{P1} - z_{P1}$). Through these plots we have inferred the photometric system correc-

tion terms via linear fits of the stellar loci. The color conversions are the following:

$$\begin{aligned}
i_{\rm GROND} &= i_{\rm P1} - 0.089 \times (r_{\rm P1} - i_{\rm P1}) + 0.001 \\
z_{\rm GROND} &= z_{\rm P1} - 0.214 \times (z_{\rm P1} - y_{\rm P1}) \\
J_{\rm GROND} &= J_{\rm 2M} - 0.012 \times (J_{\rm 2M} - H_{\rm 2M}) + 0.004 \\
H_{\rm GROND} &= H_{\rm 2M} + 0.030 \times (H_{\rm 2M} - K_{\rm 2M}) + 0.009 \\
I_{\rm EFOSC2} &= i_{\rm P1} - 0.149 \times (i_{\rm P1} - z_{\rm P1}) - 0.001 \\
Z_{\rm EFOSC2} &= z_{\rm P1} - 0.265 \times (z_{\rm P1} - y_{\rm P1}) \\
z_{\rm O2000} &= z_{\rm P1} - 0.245 \times (z_{\rm P1} - y_{\rm P1}) \\
Y_{\rm O2000} &= y_{\rm P1} - 0.413 \times (z_{\rm P1} - y_{\rm P1}) + 0.012 \\
J_{\rm O2000} &= J_{\rm 2M} + 0.093 \times (J_{\rm 2M} - H_{\rm 2M})
\end{aligned}$$

where $J_{\rm 2M}$, $H_{\rm 2M}$, and $K_{\rm 2M}$ are 2MASS magnitudes in the AB system. The accuracy of the photometric zero points was typically 0.01 – 0.04 mag and are included in the magnitude errors presented in this work.

2.7. *Spectroscopic Follow-up*

In order to confirm the nature and redshifts of the candidates, we have carried out optical and NIR spectroscopy using EFOSC2 at the NTT telescope in La Silla, the FOcal Reducer/low dispersion Spectrograph 2 (FORS2; Appenzeller & Rupprecht 1992) at the Very Large Telescope (VLT), the Multi-Object Double Spectrograph (MODS; Pogge et al. 2010) at the Large Binocular Telescope (LBT), and the Folded-port InfraRed Echellette (FIRE; Simcoe et al. 2008, 2013) spectrometer in the Baade Telescope at Las Campanas Observatory. The details of the spectroscopy observations of the new PS1 quasars are shown in Table 1. The data reduction included bias subtraction, flat fielding using lamp flats and sky subtraction. For the wavelength calibration exposures of He, HgCd and Ne arc lamps were obtained. The wavelength calibration was checked using sky emission lines. The typical rms of the wavelength calibration was better than 0.5 Å. For the flux calibrations we used observations of the spectrophotometric standard stars G158-100, GD50, LTT7379, HD49798, EG274, and G191-B2B (Oke 1990; Hamuy et al. 1992, 1994).

3. EIGHT NEW QUASARS AT REDSHIFT ~ 6

3.1. *Spectra*

We have taken spectra of nine objects that were photometrically followed up. Eight of them satisfied our criteria in Section 2.1 and they all turned out to be quasars at $z \sim 6$. One object, selected with preliminary criteria, was found to be an M-star, however this source did not satisfy the final color cuts presented in this paper. None of the eight quasars is detected in the NRAO VLA Sky Survey (Condon et al. 1998). Only PSO J007.0273+04.9571 and PSO J187.3050+04.3243 are located in the region covered by the Faint Images of the Radio Sky at Twenty cm (FIRST) radio survey (Becker et al. 1995) but they are undetected. Four quasars, PSO J340.2041–18.6621, PSO J007.0273+04.9571, PSO J037.9706–28.8389, and PSO J183.2991–12.7676, are in the *WISE* All-Sky data release products catalog (Cutri et al. 2012) with $> 3.0\sigma$ detections. The *WISE* magnitudes are tabulated in Table 7 in Appendix C.

The PS1 stacked catalog and the follow-up photometry of the quasars are presented in Tables 2 and 3. The optical spectra of the new quasars are shown in Figure 2. Each spectrum has been scaled to the corresponding $z_{\rm P1}$ magnitude. For completeness, the first PS1 quasar PSO J215.1514–16.0417 (Morganson et al. 2012) is also included in Figure 2 and Table 2.

3.2. *Redshift Determination*

There are four quasars, PSO J340.2041–18.6621, PSO J037.9706–28.8389, PSO J187.3050+04.3243, and PSO J213.3629–22.5617 that show clear emission lines and their redshift estimation was performed by Gaussian fitting to the N V, λ1240 (hereafter N V), O I + Si II λ1305 (hereafter O I + Si II), and/or Si IV + O IV] λ1398 (hereafter Si IV + O IV]) lines. The observed wavelengths in the composite spectra from Vanden Berk et al. (2001) were taken as reference. The uncertainties in our line fittings were negligible compared to the intrinsic shifts known to exist with respect to the quasar systemic redshift (Richards et al. 2002; Shen et al. 2007). Thus, following previous studies (e.g., Fan et al. 2006b; Jiang et al. 2009; Willott et al. 2009), we adopted redshift uncertainties of $\Delta z = 0.02$. The other four quasars, PSO J007.0273+04.9571, PSO J183.2991–12.7676, PSO J210.8722–12.0094, and PSO J045.1840–22.5408 have discovery spectra with a bright continuum almost devoid of bright emission lines (see Figure 2). In the absence of strong lines, an accurate redshift estimate for these quasars is challenging. We estimated their redshift by matching their continuum to the composite spectra from Vanden Berk et al. (2001) and Fan et al. (2006b). For the brightest of these quasars, PSO J183.2991–12.7676, we obtained a second spectrum with a higher S/N and extended wavelength coverage from which we were able to estimate its redshift by fitting weak emission lines. The redshift estimated by the Gaussian fitting was off by 0.03 with respect to our preliminary estimation based on the continuum matching (for more details see Section 3.3.6). Based on the case of PSO J183.2991–12.7676, we adopted a redshift uncertainty of $\Delta z = 0.05$ for the quasars whose redshifts were determined only by matching their continuum to templates. Once the redshifts were estimated, we calculated the absolute magnitude of the continuum rest frame 1450 Å (M_{1450}) for each quasar, by fitting a power law of the form $f_\lambda = C \times \lambda^\beta$ to regions of the continuum that are generally uncontaminated by emission lines (1285–1295, 1315–1325, 1340–1375, 1425–1470, 1680–1710, 1975–2050, and 2150–2250 Å) and that were not affected by significant errors or absorption features. The M_{1450} values are listed in Table 2.

3.3. *Notes on Individual Objects*

We here discuss the individual quasars, sorted by descending redshift.

3.3.1. *PSO J340.2041–18.6621 ($z = 6.00 \pm 0.02$)*

This quasar was selected from a preliminary small region of the PS1 stacked catalog. Because of the low S/N of its EFOSC2 discovery spectrum, it was difficult to determine an accurate redshift. Thus, we have obtained a higher S/N spectrum using MODS at the LBT (see Table 1). The MODS spectrum is shown in Figure 2. The

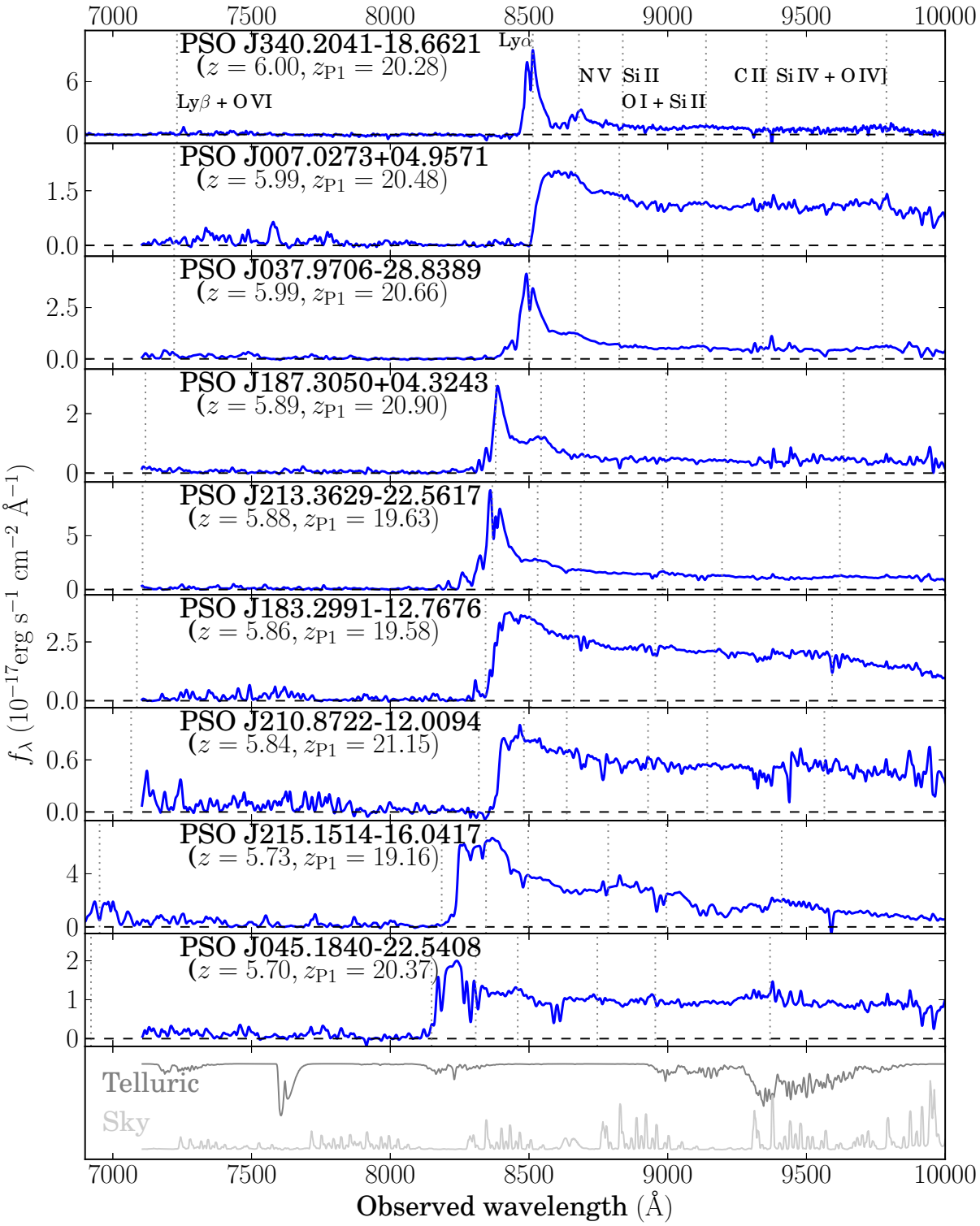

Figure 2. Spectra of the nine newly discovered PS1 quasars at $5.70 \leq z \leq 6.00$. The quasar PSO J215.1514–16.0417 was published in Morganson et al. (2012). Here we show the discovery spectra of the new quasars (with the exception of PSO J340.2041–18.6621 whose EFOSC2 discovery spectrum had very low S/N). The bottom panel shows the median telluric absorption and sky emission lines. Vertical dashed lines indicate the observed wavelengths of key spectral lines, as given in the top panel.

Table 1
Spectroscopic Observations of the New PS1 Quasars

QSO	Instrument	Date	Slit Width (arcsec)	Exp. Time (s)	Seeing (arcsec)
PSO J340.2041–18.6621	EFOSC2	2012 Jun 21	1.5	3600	0.80 – 1.40
	MODS	2012 Nov 17	1.2	3000	0.90 – 1.30
PSO J007.0273+04.9571	FORS2	2013 Jul 9	1.3	1782	0.75 – 1.01
PSO J037.9706–28.8389	FORS2	2013 Mar 4-5	1.3	3600	0.66 – 0.90
PSO J187.3050+04.3243	FORS2	2013 Apr 12	1.3	2682	1.05 – 1.17
PSO J213.3629–22.5617	FORS2	2013 May 3	1.3	1782	0.56 – 0.61
PSO J183.2991–12.7676	FORS2	2013 Apr 13	1.3	1782	0.62 – 0.77
	FIRE	2013 Apr 19	0.6	6000	0.67 – 1.22
PSO J210.8722–12.0094	FORS2	2013 May 9	1.3	2682	0.66 – 0.71
PSO J045.1840–22.5408	FORS2	2013 Aug 9	1.3	1782	0.82 – 0.90

spectrum shows a strikingly strong and narrow Lyα emission line. A separate narrow N V line is evident and the O I + Si II line is also detected. The redshift was calculated from the average of the Gaussian fits to the N V and O I + Si II lines. We have also carried out 870 μm observations of PSO J340.2041–18.6621, however the quasar remained undetected in the map with an rms of 1.6 mJy at the quasar position. Details of the submillimeter observations can be found in Appendix B.

3.3.2. *PSO J007.0273+04.9571 ($z = 5.99 \pm 0.05$)*

The discovery spectrum shows a weak-line emission quasar and with the current S/N there are not clear emission lines from which the redshift could be determined. The redshift estimate was calculated by fitting the continuum to the composite spectra from Vanden Berk et al. (2001) and Fan et al. (2006b). This quasar was independently discovered by L. Jiang et al. (in preparation).

3.3.3. *PSO J037.9706–28.8389 ($z = 5.99 \pm 0.02$)*

The discovery spectrum shows a bright Lyα line and a well separated N V line. The O I + Si II emission line is also detected. The redshift was estimated as the average of the best-fit values of the N V and O I + Si II lines.

3.3.4. *PSO J187.3050+04.3243 ($z = 5.89 \pm 0.02$)*

Bright and narrow Lyα and N V emission lines are clear in the discovery spectrum. There is a tentative Si IV + O IV] emission line but at very low S/N and in a region with considerable telluric absorption. The redshift was calculated from the Gaussian fitting to the N V emission line.

3.3.5. *PSO J213.3629–22.5617 ($z = 5.88 \pm 0.02$)*

Bright Lyα and N V emission lines are evident in the discovery spectrum. The Si IV + O IV] and O I + Si II emission lines are also detected. The redshift estimation was calculated from the best-fit values of the N V and Si IV + O IV] lines. Even though adding the fit of the O I + Si II line to the redshift determination did not change the estimated value, we decided to not consider it since it seemed to be affected by an absorption system. We identify a possible absorption system at $z = 4.780 \pm 0.002$ from the C IV $\lambda\lambda$1548, 1550 absorption feature at $\lambda = (8945.9\,\text{Å}, 8960.2\,\text{Å})$. However, we note that the scatter between the expected and observed positions of the two lines is large ($\sim$ 1 Å). The spectrum shows also a clear Mg II $\lambda\lambda$2796, 2803 absorption doublet at $\lambda = (9113.0\,\text{Å}, 9136.3\,\text{Å})$, corresponding to an absorber at $z = 2.2594 \pm 0.0005$. This absorber is further confirmed by the presence at the same redshift of the Fe II λ2586 absorption at $\lambda = 8429.8$ and Fe II λ2600 Å absorption at $\lambda = 8474.0$ Å.

3.3.6. *PSO J183.2991–12.7676 ($z = 5.86 \pm 0.02$)*

This is the brightest quasar in our new sample (but fainter than PSO J215.1514–16.0417 reported in Morganson et al. 2012). Figure 2 shows the FORS2 discovery spectrum. This spectrum has a very bright continuum but it does not show any detectable emission line and it seems that Lyα is almost completely absorbed. Since we did not have emission lines to fit, we estimated a preliminary redshift from fitting the continuum to the composite spectra from Vanden Berk et al. (2001) and Fan et al. (2006b), yielding $z = 5.83$. We obtained a second spectrum of higher S/N of this object using the FIRE spectrometer (see Table 1). The FIRE spectrum was scaled to the $y_{\rm P1}$ magnitude and is presented in Figure 3. The spectrum shows clear O I + Si II and Si IV + O IV] emission lines which were used for the final redshift estimation. The O I + Si II and Si IV + O IV] lines are affected by absorption systems, but the signal is high enough to get good fits even when masking the absorbed regions. There is a tentative C II emission line at lower S/N also affected by absorption that was not used for the redshift estimate. In the case of this quasar, the redshift estimated by matching the continuum was off by 0.03 with respect to the line fitting estimate ($z = 5.86$). Based on this case, we assumed a redshift uncertainty of 0.05 for the other weak-line emission quasars in our sample whose redshift estimate was solely based on continuum fitting. We identify absorptions systems at $z = 4.460 \pm 0.002$, $z = 2.1074 \pm 0.0005$, and $z = 2.431 \pm 0.001$ from the C IV $\lambda\lambda$1548, 1550 doublet at $\lambda = (8946.2\,\text{Å}, 8961.3\,\text{Å})$, Mg II $\lambda\lambda$2796, 2803 doublet at $\lambda = (8688.5\,\text{Å}, 8709.8\,\text{Å})$, and another Mg II $\lambda\lambda$2796, 2803 doublet at $\lambda = (9593.4\,\text{Å}, 9618.6\,\text{Å})$ respectively. For the latter we also identify the associated Fe II λ2586 absorption at $\lambda = 8874.8$ and the Fe II λ2600 Å absorption at $\lambda = 8921.3$ Å. There seems to be a broad absorption line blueshifted from the expected location of the C IV λ1546 (hereafter C IV) emission line, which is remarkably absorbed in the spectrum of this quasar.

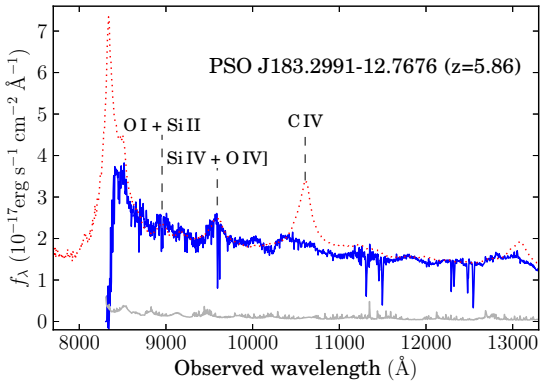

Figure 3. FIRE spectrum of the quasar PSO J183.2991–12.7676 ($z = 5.86$). The gray solid line around zero flux shows the 1σ error. The dotted line shows the composite spectrum from Vanden Berk et al. (2001) as reference. Unlike the discovery spectrum in Figure 2, the O I + Si II and Si IV + O IV] emission lines are clearly identified.

3.3.7. *PSO J210.8722–12.0094 ($z = 5.84 \pm 0.05$)*

This is the faintest of the PS1 quasar sample ($z_{\rm P1} = 21.15 \pm 0.08$). The discovery spectrum does not have a S/N high enough to identify clear features in the quasar, it seems rather a weak-line emission or lineless quasar. The redshift estimate had to be determined by fitting the continuum to the composite spectra of Vanden Berk et al. (2001) and Fan et al. (2006b). There seems to be a weak absorption feature at $\lambda\lambda = 8692.6, 8705.3$. If real, it could be associated with a C IV $\lambda\lambda$1548, 1550 absorption system at $z = 4.616 \pm 0.001$,

although with the current S/N it is hard to tell.

3.3.8. *PSO J045.1840–22.5408 ($z = 5.70 \pm 0.05$)*

This is the lowest redshift quasar in the PS1 sample so far. The discovery spectrum of this quasar looks very peculiar and seems to be significantly affected by absorption systems or intrinsic absorption from the host galaxy. The spectrum shows a weak-line emission quasar and the S/N does not allow us to identify emission lines in regions not affected by significant telluric absorption or sky emission to calculate the redshift from. The redshift was estimated by matching the continuum to the composite spectra from Vanden Berk et al. (2001) and Fan et al. (2006b). There are tentative Si II and Si IV + O IV] emission lines. If real, the redshift estimated from the average of their Gaussian fits correspond to $z = 5.69$, in agreement with our continuum fitting. However, we conservatively estimated the redshift uncertainty as $\Delta z = 0.05$ as for the other weak emission line quasars where the redshift was calculated only from continuum matching. There are also several absorption lines around 8300 Å (e.g., $\lambda = 8265.2$, 8281.3, 8306.8, and 8315.6 Å). Most of the lines are blended and, given the resolution of the spectrum, it is hard to unambiguously identify them. These lines could be due to a group of galaxies at $z \sim 1.96$ if we assume that all the lines are due to Mg II absorbers. We identify a Mg II $\lambda\lambda 2796, 2803$ doublet at $z = 2.0721 \pm 0.0005$ (observed at $\lambda = 8589.2$ Å and 8611.9 Å). The corresponding Mg I $\lambda 2853$ Å seems marginally detected at $\lambda = 8764.0$ Å.

4. KNOWN QUASARS IN Pan-STARRS1

As mentioned in Section 2.5, the 17 known quasars in Table 4 and PSO J215.1514–16.0417 in Table 2 were part of our candidate list. In order to calculate the fraction of known quasars that we recover using our current selection strategy, we cross-matched a list of the known quasars at $z > 5.7$ with our PS1 stacked catalog. We required the quasars to satisfy the same criteria as in Section 2 except for the magnitude and color cuts (Equations (1a), (1d), (1e), (1f), and (1g)). In our current catalog, there are 36 known quasars that satisfy these criteria, including the quasars discovered in this work. Other quasars do not appear in our catalog for a variety of reasons including (1) they are detected in PS1 but flagged or not detected in at least one of the bands in which we are requiring detections ($i_{\rm P1}$, $z_{\rm P1}$, and $y_{\rm P1}$), (2) they are in regions without coverage i.e., chip gaps, quasars with $92^\circ <$ R.A. $< 132^\circ$ (our catalog has no coverage at this R.A. range), or quasars with Decl. $< -30^\circ$; (3) they are too faint for the current depth of PS1 (i.e., S/N($z_{\rm P1}$)< 10 or S/N($y_{\rm P1}$)< 5). The PS1 colors of published quasars and the unpublished quasars from S.J. Warren et al. (in preparation) are shown in Figure 1 with blue squares and green triangles respectively. Table 5 shows the PS1 photometry of the known quasars that are in the PS1 catalog but do not satisfy our color selection. In total, we are recovering 72% (26/36) of the high-redshift quasars detected in PS1. Among the known quasars that do not pass our color criteria are SDSSJ1148+5251 ($z = 6.42$) and ULASJ1148+0702 ($z = 6.29$) which are not strictly speaking part of our $z \sim 6$ search, they have $z_{\rm P1} - y_{\rm P1} > 0.5$ and lower limits in the $i_{\rm P1} - z_{\rm P1}$ color. SDSSJ1048+4637 ($z = 6.20$) and ULASJ1319+0950 ($z = 6.133$) have very quasar-like colors ($i_{\rm P1} - z_{\rm P1} = 2.79$ and $z_{\rm P1} - y_{\rm P1} = 0.70$; and $i_{\rm P1} - z_{\rm P1} = 2.42$ and $z_{\rm P1} - y_{\rm P1} = 0.61$ respectively) and would be selected as quasars in our next search at higher redshifts (where we will allow $z_{\rm P1} - y_{\rm P1} > 0.5$). CFHQSJ1509–1749 ($z = 6.12$) has only a lower limit of $i_{\rm P1} - z_{\rm P1} > 1.81$ and $z - y = 0.64$, it could be detected as a quasar in our $z > 6.2$ search if the $i_{\rm P1}$-band goes deeper in the next release of the stacked catalog. SDSSJ2310+1855 ($z = 6.0031$) has $i_{\rm P1} - z_{\rm P1} = 1.91$ and $z_{\rm P1} - y_{\rm P1} = 0.56$ colors and will not be selected in our next searches because its colors are in a region with high contamination of brown dwarfs. SDSSJ0353+0104 with colors $i_{\rm P1} - z_{\rm P1} > 1.97$ and $z_{\rm P1} - y_{\rm P1} = 0.46$ is barely missed by our selection and will be likely selected as a quasar when the depth of the $i_{\rm P1}$ band increases. SDSSJ2054–0005 ($z = 6.0391$), SDSSJ0927+2001 ($z = 5.77$), and SDSSJ1621+5155 ($z = 5.71$) are missed by our selection because their PS1 colors are hard to distinguish from the more abundant brown dwarfs. Using our current criteria for $z \sim 6$ quasars we estimate that we recover $\sim 81\%$ (17/21) of the quasars that we are supposed to find ($z - y < 0.5$, excluding the PS1 quasars). With this work, PS1 has discovered more than 10% of the $z > 5.7$ quasars published thus far. Figure 4 shows the redshift distribution of all the $z \geq 5.7$ quasars published to date, highlighting the discovery surveys.

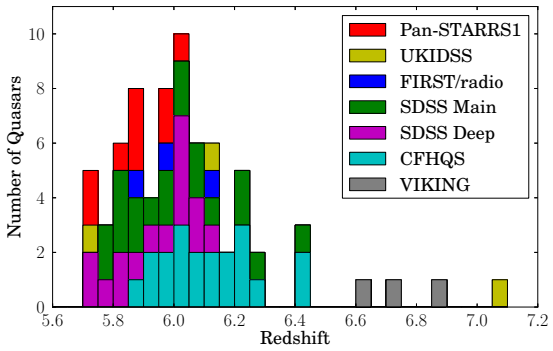

Figure 4. Redshift distribution of the $z \geq 5.7$ quasars published to date. Pan-STARRS1 includes the quasars in Morganson et al. (2012) and this work. UKIDSS includes the quasars in Venemans et al. (2007) and Mortlock et al. (2009, 2011). FIRST/radio includes the quasars in McGreer et al. (2006), Cool et al. (2006), and Zeimann et al. (2011). SDSS Main includes the quasars in Fan et al. (2001, 2003, 2004, 2006b). SDSS Deep includes the quasars in Mahabal et al. (2005), Goto (2006), Jiang et al. (2008), Wang et al. (2008), Jiang et al. (2009), De Rosa et al. (2011), and Wang et al. (2013). CFHQS includes the quasars in Willott et al. (2007, 2009, 2010b,a). VIKING includes the quasars in Venemans et al. (2013).

5. HOW COMMON ARE WEAK EMISSION LINE QUASARS?

Weak-line quasars are rare objects characterized by a flat continuum and the lack of strong emission lines. Meusinger et al. (2012) selected a sample of $\sim$ 1000 quasars ($0.6 < z < 4.3$) with unusual spectra from the SDSS DR7. From these peculiar objects, they found that 18% were weak-line quasars. Diamond-Stanic et al. (2009) studied the SDSS DR5 quasar catalog and defined weak-line quasars as the ones that have the rest-frame equivalent-width (EW) of the Lyα+N V line (determined between $\lambda_{\rm rest} = 1160$ Å and $\lambda_{\rm rest} = 1290$ Å) lower than 15.4 Å. They showed that the frac-

Table 2
PS1 Stacked Catalog Magnitudes, Redshifts, and Absolute Magnitudes of the PS1 High-redshift Quasars.

QSO	R.A. (J2000)	Decl. (J2000)	$i_{\rm P1}$[a]	$z_{\rm P1}$	$y_{\rm P1}$	Redshift	M_{1450}
PSO J340.2041–18.6621	22:40:48.98	–18:39:43.8	> 23.44	20.28 ± 0.05	20.47 ± 0.13	6.00	-26.0
PSO J007.0273+04.9571	00:28:06.56	+04:57:25.7	23.24 ± 0.29	20.48 ± 0.06	20.18 ± 0.08	5.99	-26.5
PSO J037.9706–28.8389	02:31:52.96	–28:50:20.1	> 22.76	20.66 ± 0.09	20.70 ± 0.21	5.99	-25.6
PSO J187.3050+04.3243	12:29:13.21	+04:19:27.7	23.19 ± 0.28	20.90 ± 0.05	21.09 ± 0.18	5.89	-25.4
PSO J213.3629–22.5617	14:13:27.12	–22:33:42.3	22.98 ± 0.34	19.63 ± 0.04	19.83 ± 0.11	5.88	-26.6
PSO J183.2991–12.7676	12:13:11.81	–12:46:03.5	22.32 ± 0.15	19.58 ± 0.04	19.31 ± 0.05	5.86	-27.3
PSO J210.8722–12.0094	14:03:29.33	–12:00:34.1	> 23.17	21.15 ± 0.08	20.69 ± 0.13	5.84	-25.7
PSO J215.1514–16.0417[b]	14:20:36.34	–16:02:30.2	21.75 ± 0.09	19.16 ± 0.02	19.17 ± 0.08	5.73	-27.6[c]
PSO J045.1840–22.5408	03:00:44.18	–22:32:27.2	> 22.79	20.37 ± 0.06	20.53 ± 0.15	5.70	-26.4

[a]The lower limits correspond to 3σ limiting magnitudes.
[b]Quasar published in Morganson et al. (2012), here we have slightly modified the coordinates from PSO J215.1512-16.0417 to PSO J215.1514–16.0417 based on the stacked catalog.
[c]To calculate this absolute magnitude, we took the best continuum fit from Morganson et al. (2012) and scaled it to the $z_{\rm P1}$ stack magnitude presented here.

Table 3
Follow-up Photometry of the New PS1 Quasars.

QSO	$i_{\rm GROND}$	$z_{\rm GROND}$	$J_{\rm GROND}$	$H_{\rm GROND}$	$I_{\rm EFOSC2}$	$Z_{\rm EFOSC2}$
PSO J340.2041–18.6621	23.32 ± 0.17	20.11 ± 0.04	20.28 ± 0.08	19.9 ± 0.11	···	···
PSO J007.0273+04.9571	22.74 ± 0.24	20.39 ± 0.04	19.77 ± 0.11	19.71 ± 0.15	···	···
PSO J037.9706–28.8389	23.19 ± 0.15	20.78 ± 0.04	20.41 ± 0.14	20.59 ± 0.26	···	···
PSO J187.3050+04.3243	···	···	···	···	21.85 ± 0.04	21.00 ± 0.04
PSO J213.3629–22.5617	···	···	···	···	20.70 ± 0.02	19.77 ± 0.01
PSO J183.2991–12.7676	···	···	···	···	20.69 ± 0.03	19.31 ± 0.02
PSO J210.8722–12.0094	···	···	···	···	22.35 ± 0.06	21.00 ± 0.03
PSO J045.1840–22.5408	22.78 ± 0.10	20.35 ± 0.03	19.65 ± 0.08	19.42 ± 0.08	···	···

Table 4
High-Redshift Quasars from other Surveys that were Part of the Final Candidate List in this Work.

QSO	R.A. (J2000)[a]	Decl. (J2000)[a]	$i_{\rm P1}$[b]	$z_{\rm P1}$	$y_{\rm P1}$	Redshift	Reference
SDSSJ1030+0524	10:30:27.12	+05:24:55.1	> 22.98	20.10 ± 0.05	20.28 ± 0.20	6.28	1
SDSSJ1623+3112	16:23:31.81	+31:12:00.5	> 23.27	20.20 ± 0.06	20.22 ± 0.10	6.22	1
SDSSJ1250+3130	12:50:51.91	+31:30:21.8	23.55 ± 0.39	19.94 ± 0.04	20.26 ± 0.12	6.13	1
SDSSJ1602+4228	16:02:53.95	+42:28:25.0	22.56 ± 0.20	20.09 ± 0.03	19.71 ± 0.06	6.07	1
SDSSJ1630+4012	16:30:33.90	+40:12:09.7	23.02 ± 0.35	20.37 ± 0.07	20.58 ± 0.12	6.05	1
ULASJ1207+0630	12:07:37.44	+06:30:10.2	> 23.22	20.44 ± 0.04	20.19 ± 0.11	6.04	2
SDSSJ1137+3549	11:37:17.73	+35:49:56.9	22.15 ± 0.11	19.43 ± 0.02	19.44 ± 0.05	6.01	1
ULASJ0148+0600	01:48:37.64	+06:00:20.1	22.80 ± 0.25	19.46 ± 0.02	19.40 ± 0.04	5.96	2
SDSSJ1335+3533	13:35:50.81	+35:33:15.9	22.57 ± 0.28	20.27 ± 0.03	19.97 ± 0.08	5.95	1
SDSSJ1411+1217	14:11:11.29	+12:17:37.3	23.25 ± 0.26	19.57 ± 0.02	20.08 ± 0.08	5.93	1
SDSSJ0005–0006	00:05:52.34	–00:06:55.7	23.09 ± 0.20	20.50 ± 0.06	20.69 ± 0.14	5.85	1
NDWFSJ1425+3254	14:25:16.33	+32:54:09.5	23.40 ± 0.37	20.44 ± 0.04	20.33 ± 0.11	5.85	3
ULASJ1243+2529	12:43:40.82	+25:29:23.8	> 23.51	20.18 ± 0.05	20.61 ± 0.14	5.83	2
SDSSJ1436+5007	14:36:11.73	+50:07:07.2	22.57 ± 0.23	20.24 ± 0.06	20.24 ± 0.08	5.83	1
SDSSJ0002+2550	00:02:39.39	+25:50:35.0	21.93 ± 0.08	19.02 ± 0.05	19.53 ± 0.07	5.80	1
SDSSJ1044–0125	10:44:33.04	–01:25:02.1	21.87 ± 0.12	19.35 ± 0.02	19.29 ± 0.07	5.7847	4
ULASJ0203+0012	02:03:32.38	+00:12:29.3	> 23.85	20.78 ± 0.09	20.50 ± 0.12	5.72	5

References. — (1) Fan et al. (2006c); (2) S.J. Warren et al., in preparation; (3) Cool et al. (2006); (4) Wang et al. (2013); (5) Mortlock et al. (2009)

[a]The coordinates correspond to the coordinates in the PS1 stacked catalog and are not necessarily identical to the ones in the discovery papers.
[b]The lower limits correspond to 3σ limiting magnitudes.

Table 5
High-redshift Quasars from other Surveys that did not Satisfy the Color Selection of this Work

QSO	R.A. (J2000)[a]	Decl. (J2000)[a]	$i_{\rm P1}$[b]	$z_{\rm P1}$	$y_{\rm P1}$	Redshift	Reference
SDSSJ1148+5251	11:48:16.65	+52:51:50.4	> 23.07	20.63 ± 0.04	19.42 ± 0.10	6.42	1
ULASJ1148+0702	11:48:03.29	+07:02:08.3	> 22.71	21.03 ± 0.08	20.44 ± 0.15	6.29	2
SDSSJ1048+4637	10:48:45.07	+46:37:18.5	22.98 ± 0.38	20.19 ± 0.04	19.49 ± 0.12	6.20	1
ULASJ1319+0950	13:19:11.30	+09:50:51.5	22.56 ± 0.19	20.14 ± 0.04	19.53 ± 0.07	6.1330	3
CFHQSJ1509–1749	15:09:41.78	–17:49:26.8	> 22.06	20.25 ± 0.07	19.61 ± 0.10	6.12	4
SDSSJ0353+0104	03:53:49.73	+01:04:04.7	> 23.12	21.15 ± 0.10	20.69 ± 0.19	6.049	5
SDSSJ2054–0005	20:54:06.50	–00:05:14.4	22.65 ± 0.20	21.01 ± 0.09	20.66 ± 0.17	6.0391	3
SDSSJ2310+1855	23:10:38.89	+18:55:19.9	21.55 ± 0.10	19.64 ± 0.04	19.08 ± 0.04	6.0031	2
SDSSJ0927+2001	09:27:21.82	+20:01:23.5	21.52 ± 0.16	19.86 ± 0.03	19.88 ± 0.11	5.77	6
SDSSJ1621+5155	16:21:00.94	+51:55:48.8	21.96 ± 0.14	20.05 ± 0.06	19.80 ± 0.08	5.71	7

References. — (1) Fan et al. (2006c); (2) S.J Warren et al., in preparation; (3) Wang et al. (2013); (4) Willott et al. (2007); (5) Jiang et al. (2008); (6) Carilli et al. (2007); (7) Wang et al. (2008)

[a]The coordinates correspond to the coordinates in the PS1 stacked catalog and are not necessarily identical to the ones in the discovery papers.
[a]The lower limits correspond to 3σ limiting magnitudes.

tion of weak-line quasars increased from 1.3% at $z < 4.2$ to 6.2% at $z > 4.2$. From Figure 2, we noticed that half of the quasars discovered in this paper (PSO J007.0273+04.9571, PSO J183.2991–12.7676, PSO J210.8722–12.0094, PSO J045.1840–22.5408) show a weak or absorbed Lyα line. However, following the Diamond-Stanic et al. (2009) hard-cut definition, only PSO J183.2991–12.7676 and PSO J210.8722–12.0094, belong to their weak-line quasar classification with Lyα+N v EWs of 11.8 and 10.7 Å respectively. We noted that the EW is very dependent on the continuum fit estimate and since most of our spectra do not cover the region with $\lambda_{\rm rest} > 1500$ Å, a good fit to the continuum is challenging. Thus, the uncertainties in our EW estimates are of the order of 25%. Future NIR spectra of these quasars will improve these measurements.

Even though these are low number statistics, 25% of the quasars presented in this paper are weak-line quasars, which is a higher fraction than found in lower redshift studies and is consistent with the ∼20% of weak-line quasars found in the SDSS main $z \sim 6$ quasar sample (X. Fan et al., in preparation.).

In principle, this kind of object should be easier to select at higher redshifts due to the strong Lyα forest and Lyman limit systems that produce a characteristic break in the colors of high-redshift quasars, independent of their emission lines. Thus, while high redshift searches based on colors—like this work—should be equally sensitive to both weak-line emission quasars and normal quasars, some weak-line quasars could have been missed at lower redshift due to the color-based selection criteria.

Several scenarios have been proposed to explain the existence of such weak-line objects, including that they could be strongly lensed galaxies, BL Lac objects, objects where the quasar activity has just started, or invoking unusual broad-line region properties in comparison to normal quasars (e.g., Hryniewicz et al. 2010; Shemmer et al. 2010; Lane et al. 2011). Nevertheless, no consensus has yet been reached. Recently, Laor & Davis (2011) proposed that weak-line or lineless quasars may be produced by cold accretion discs that imply non-ionizing continuum for some combinations of black hole masses and quasar luminosities. They claimed that very high masses in luminous active galactic nuclei are required in order to have a cold accretion disc ($M \gtrsim 3 \times 10^9\,{\rm M}_\odot$, $L \approx 10^{46}\,{\rm erg\ s^{-1}}$, especially for non-rotating black holes). These numbers are similar to the masses and luminosities found in $z \sim 6$ quasars (e.g., Kurk et al. 2007; De Rosa et al. 2011), so this mechanism could be a simple explanation of the high fraction of weak-line quasars in our sample. A more extensive sample of quasars is urgently needed to shed light on the nature of these objects.

6. SUMMARY

We have presented the discovery of eight new quasars at $z \sim 6$. With this work, PS1 has now discovered a total of nine quasars at $5.7 \leq z \leq 6.0$. We estimated that using the selection strategy of this paper, we recover ∼ 81% of the known quasars in our target redshift range (excluding the PS1 quasars). The others are missed because their PS1 colors are hard to distinguish from brown dwarfs. Follow-up observations are still on-going and the discovery of more quasars is expected, therefore conclusions on the luminosity function and the space density of $z \sim 6$ quasars are not possible at this time. The variety of spectral features among these quasars is remarkable, including four quasars with very bright emission lines and another four quasars with almost no detectable emission lines. The fraction of weak-line emission quasars found in this work (25%) is much larger than fractions found by other studies at lower redshifts (e.g., Diamond-Stanic et al. 2009) but consistent with the fraction in the SDSS main $z \sim 6$ quasar sample (X. Fan et al., in preparation). Our new discoveries show that weak-line emission quasars could be more common at the highest redshifts than previously thought.

E.B. thanks B. Goldmann for providing the PS1 colors of brown dwarfs, E. Schlafly for helpful discussions about PS1 data, N. Crighton and K. Rubin for their help with MODS data reduction, C.-H. Lee and L. Johnsen for useful comments on the paper, and the IMPRS for Astronomy & Cosmic Physics at the University of Heidelberg. XF and IM acknowledge support from NSF grant AST 08-06861 and AST 11-07682.

The Pan-STARRS1 Surveys (PS1) have been made possible through contributions of the Institute for Astronomy, the University of Hawaii, the Pan-STARRS Project Office, the Max-Planck Society and its participating institutes, the Max Planck Institute for Astronomy, Heidelberg and the Max Planck Institute for Extraterrestrial Physics, Garching, The Johns Hopkins University, Durham University, the University of Edinburgh, Queen's University Belfast, the Harvard-Smithsonian Center for Astrophysics, the Las Cumbres Observatory Global Telescope Network Incorporated, the National Central University of Taiwan, the Space Telescope Science Institute, the National Aeronautics and Space Administration under grant No. NNX08AR22G issued through the Planetary Science Division of the NASA Science Mission Directorate, the National Science Foundation under grant No. AST-1238877, the University of Maryland, and Eotvos Lorand University (ELTE).

This work is based on observations made with ESO Telescopes at the La Silla Paranal Observatory under programmes ID 088.A-0119, 088.A-9004, 089.A-0290, 090.A-0383, 090.A-0642, and 091.A-0421.

The LBT is an international collaboration among institutions in the United States, Italy and Germany. The LBT Corporation partners are: The University of Arizona on behalf of the Arizona university system; Istituto Nazionale di Astrofisica, Italy; LBT Beteiligungsgesellschaft, Germany, representing the Max Planck Society, the Astrophysical Institute Potsdam, and Heidelberg University; The Ohio State University; The Research Corporation, on behalf of The University of Notre Dame, University of Minnesota and University of Virginia.

This paper used data obtained with the MODS spectrographs built with funding from NSF grant AST-9987045 and the NSF Telescope System Instrumentation Program (TSIP), with additional funds from the Ohio Board of Regents and the Ohio State University Office of Research.

Part of the funding for GROND (both hardware as well as personnel) was generously granted from the Leibniz-Prize to Prof. G. Hasinger (DFG grant HA 1850/28-1).

We acknowledge the use of the Calar Alto Faint Object Spectrograph at the 2.2m telescope (CAFOS) and MMT/SWIRC, for follow-up of some of the early PS1 candidates.

Based on observations collected at the Centro Astronómico Hispano Alemán (CAHA) at Calar Alto, operated jointly by the Max-Planck Institut für Astronomie and the Instituto de Astrofísica de Andalucía (CSIC)'

Observations reported here were obtained at the MMT Observatory, a joint facility of the University of Arizona and the Smithsonian Institution.

This paper includes data gathered with the 6.5 meter Magellan Telescopes located at Las Campanas Observatory, Chile.

This publication makes use of data products from the Two Micron All Sky Survey, which is a joint project of the University of Massachusetts and the Infrared Processing and Analysis Center/California Institute of Technology, funded by the National Aeronautics and Space Administration and the National Science Foundation.

Funding for SDSS-III has been provided by the Alfred P. Sloan Foundation, the Participating Institutions, the National Science Foundation, and the U.S. Department of Energy Office of Science. The SDSS-III web site is http://www.sdss3.org/.

SDSS-III is managed by the Astrophysical Research Consortium for the Participating Institutions of the SDSS-III Collaboration including the University of Arizona, the Brazilian Participation Group, Brookhaven National Laboratory, University of Cambridge, Carnegie Mellon University, University of Florida, the French Participation Group, the German Participation Group, Harvard University, the Instituto de Astrofisica de Canarias, the Michigan State/Notre Dame/JINA Participation Group, Johns Hopkins University, Lawrence Berkeley National Laboratory, Max Planck Institute for Astrophysics, Max Planck Institute for Extraterrestrial Physics, New Mexico State University, New York University, Ohio State University, Pennsylvania State University, University of Portsmouth, Princeton University, the Spanish Participation Group, University of Tokyo, University of Utah, Vanderbilt University, University of Virginia, University of Washington, and Yale University.

This publication makes use of data products from the *Wide-field Infrared Survey Explorer*, which is a joint project of the University of California, Los Angeles, and the Jet Propulsion Laboratory/California Institute of Technology, funded by the National Aeronautics and Space Administration.

This research made use of Astropy, a community-developed core Python package for Astronomy (Astropy Collaboration et al. 2013, `http://www.astropy.org`). This publication made use of TOPCAT (Taylor 2005, `http://www.starlink.ac.uk/topcat`) and STILTS (Taylor 2006, `http://www.starlink.ac.uk/stilts`). The plots in this publication were produced using Matplotlib (Hunter 2007, `http://www.matplotlib.org`).

Facilities: PS1 (GPC1),VLT:Antu (FORS2), NTT (EFOSC2), LBT (MODS), Magellan:Baade (FIRE), CAO:3.5m (Omega2000), CAO:2.2m (CAFOS), Max Planck:2.2m (GROND), MMT (SWIRC)

APPENDIX

A. PAN-STARRS1 LOW-QUALITY FLAGS

Here we present Table 6, containing the PS1 flags used in our selection.

B. PSO J340.2041–18.6621 SUBMILLIMETER OBSERVATIONS

The far-infrared (FIR) emission traces the warm dust emission from quasar host galaxies and allows us to estimate their star formation rates. Studies from $z \sim 6$ quasars have shown that $\sim 30\%$ of these quasars are bright at millimeter and submillimeter wavelengths (e.g., Wang et al. 2008). With this in mind, we took 870 μm observations of PSO J340.2041–18.6621 using the Large APEX Bolometer Camera (LABOCA; Siringo et al. 2009) on the 12 m APEX telescope (Güsten et al. 2006). The observations were carried out during 2012 November for a total of 14.5 hr. The quasar was observed mainly in the afternoon or early evening in mediocre to poor weather conditions. The data were reduced using the standard procedures implemented in the BoA software (Schuller 2012). The quasar remained undetected in the map with an rms of 1.6 mJy at the quasar position. In the same map, however, we detected a tentative 4.7σ submillimeter source. Its coordinates are R.A.= 22:40:59.407 and Decl.=-18:39:34.94. It is located at a distance of $\sim 2.''5$ from PSO J340.2041–18.6621 and we did not find an evident optical counterpart. The 870 μm flux of this serendipitous source is 9.50 ± 2.02 mJy. Figure 5 shows the 870 μm 1σ-contours overlaid over the $J_{\rm GROND}$ image.

C. *WISE* MAGNITUDES

We cross-matched the PS1 quasars from Table 2 with the *WISE* All-Sky data release products catalog (Cutri et al. 2012) within a radius of $3''$. Three quasars were detected in the main all-sky release source catalog with S/N > 5.0 in the W1 band and two quasars were detected in the *WISE* 'Reject Table' [13] with S/N > 3.0 in the W1 band. The *WISE* photometry is presented in Table 7. For completeness, in Table 7 we also included the *WISE* photometry for the *WISE*-detected quasars from Tables 4 and 5.

REFERENCES

Aihara, H., Allende Prieto, C., An, D., et al. 2011, ApJS, 193, 29

[13] `http://wise2.ipac.caltech.edu/docs/release/allsky/expsup/sec2_4a.html`

Table 6
Pan-STARRS1 Bit-flags Used to Exclude Bad or Low-quality Detections.

FLAG1 NAME	**Hex Value**	**Description**
FITFAIL	0x00000008	Fit (nonlinear) failed (non-converge, off-edge, run to zero)
POORFIT	0x00000010	Fit succeeds, but low-SN or high-Chisq
PAIR	0x00000020	Source fitted with a double psf
SATSTAR	0x00000080	Source model peak is above saturation
BLEND	0x00000100	Source is a blend with other sources
BADPSF	0x00000400	Failed to get good estimate of object's PSF
DEFECT	0x00000800	Source is thought to be a defect
SATURATED	0x00001000	Source is thought to be saturated pixels (bleed trail)
CR_LIMIT	0x00002000	Source has crNsigma above limit
EXT_LIMIT	0x00004000	Source has extNsigma above limit
MOMENTS_FAILURE	0x00008000	Could not measure the moments
SKY_FAILURE	0x00010000	Could not measure the local sky
SKYVAR_FAILURE	0x00020000	Could not measure the local sky variance
MOMENTS_SN	0x00040000	Moments not measured due to low S/N
BLEND_FIT	0x00400000	Source was fitted as a blend
SIZE_SKIPPED	0x10000000	Size could not be determined
ON_SPIKE	0x20000000	Peak lands on diffraction spike
ON_GHOST	0x40000000	Peak lands on ghost or glint
OFF_CHIP	0x80000000	Peak lands off edge of chip
FLAG2 NAME	**Hex Value**	**Description**
ON_SPIKE	0x00000008	$> 25\%$ of pixels land on diffraction spike
ON_STARCORE	0x00000010	$> 25\%$ of pixels land on star core
ON_BURNTOOL	0x00000020	$> 25\%$of pixels land on burntool subtraction region

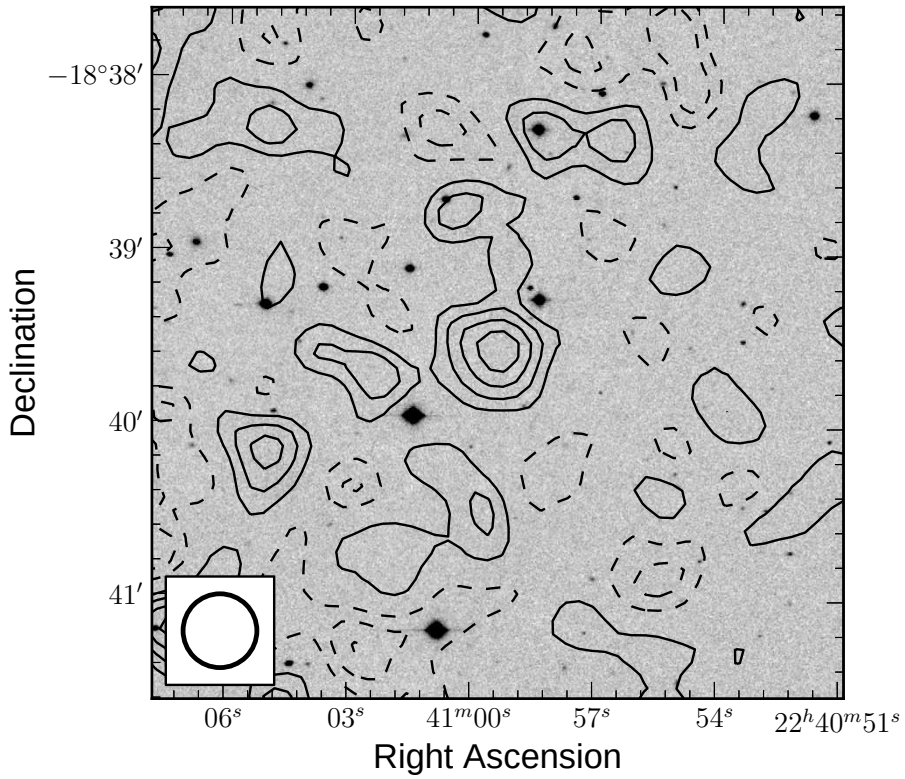

Figure 5. Image centered on the serendipitous 870 μm source at a distance of 2.′5 from PSO J340.2041–18.6621 (outside the image). The solid (dashed) lines are the positive (negative) 1σ-contours overlaid over the $J_{\rm GROND}$ image. The detection is 9.50 ± 2.02 mJy. There is no evident optical counterpart. The LABOCA beam size of 18.″2 × 18.″2 is shown in the bottom left panel.

Table 7
WISE Magnitudes for *WISE*-detected Quasars from Table 2 (the five entries at the top), Table 4 (the 17 entries in the middle), and Table 5 (the nine entries at the bottom).

QSO	W1	σ_1	W2	σ_2	W3	σ_3	W4	σ_4	Table[a]
PSO J340.2041–18.6621	16.744	0.143	15.851	0.231	12.555	...	9.060	...	M
PSO J007.0273+04.9571	17.606	0.286	16.194	0.310	12.403	...	8.628	...	R
PSO J037.9706–28.8389	18.025	0.339	16.454	...	12.913	...	8.995	...	R
PSO J183.2991–12.7676	16.387	0.098	16.323	0.310	12.710	...	8.625	...	M
PSO J215.1514–16.0417	15.567	0.047	14.778	0.068	11.782	0.205	8.758	0.329	M
SDSSJ1030+0524[b]	16.512	0.114	15.567	0.174	12.364	...	8.372	...	M
SDSSJ1623+3112[b]	16.839	0.110	15.914	0.166	12.706	...	9.268	...	M
SDSSJ1250+3130[b]	16.489	0.096	15.474	0.136	12.302	...	8.473	...	M
SDSSJ1602+4228[b]	16.107	0.046	15.209	0.062	12.184	0.184	9.526	...	M
SDSSJ1630+4012[b]	18.000	0.271	17.138	...	13.122	...	9.447	...	R
ULASJ1207+0630	17.217	0.209	16.005	0.265	12.514	...	8.442	...	M
SDSSJ1137+3549[b]	16.379	0.092	15.868	0.193	12.144	...	8.765	...	M
ULASJ0148+0600	16.200	0.066	15.267	0.099	12.753	...	8.728	...	M
SDSSJ1335+3533	16.936	0.126	15.944	0.170	12.756	...	9.405	...	M
SDSSJ1411+1217	16.709	0.088	15.612	0.107	13.014	...	9.375	...	M
SDSSJ0005–0006	17.707	0.319	16.827	...	12.368	...	8.359	...	R
NDWFSJ1425+3254	17.147	0.144	16.607	0.241	13.288	...	9.083	...	M
ULASJ1243+2529	16.72	0.144	15.594	0.149	12.826	...	9.229	...	M
SDSSJ1436+5007	17.541	0.165	16.771	0.271	13.203	...	9.532	...	M
SDSSJ0002+2550	16.330	0.078	15.410	0.147	12.012	0.259	8.579	...	M
SDSSJ1044–0125	16.274	0.088	15.546	0.155	12.281	0.362	9.532	...	M
ULASJ0203+0012	16.656	0.095	16.546	0.293	12.381	0.339	9.369	...	M
SDSSJ1148+5251[b]	16.007	0.062	15.242	0.093	12.544	0.350	8.598	...	M
ULASJ1148+0702	16.632	0.131	15.537	0.167	12.534	...	8.700	...	M
SDSSJ1048+4637[b]	16.430	0.080	16.259	0.233	12.885	...	8.843	...	M
ULASJ1319+0950[b]	17.222	0.145	16.848	0.400	12.966	...	9.030	...	M
SDSSJ0353+0104[b]	16.886	0.147	16.497	0.375	12.225	...	8.560	...	M
SDSSJ2054–0005[b]	18.017	0.339	16.250	...	12.595	...	8.727	...	R
SDSSJ2310+1855	15.950	0.067	15.192	0.107	12.541	...	9.003	...	M
SDSSJ0927+2001	17.134	0.205	16.776	...	11.994	...	8.423	...	M
SDSSJ1621+5155	15.711	0.036	14.782	0.043	13.033	0.293	9.609	...	M

A detection is considered when a S/N greater than 3.0 in the W1 band is reported. Error values are only listed when S/N> 3.0; otherwise null results (...) are listed.
[a]The *WISE* table where the quasar information are found. M: Main *WISE* all-sky release source catalog. R: *WISE* Reject Table.
[b]The *WISE* magnitudes for these quasars were also reported by Blain et al. (2013).

Appenzeller, I., & Rupprecht, G. 1992, The Messenger, 67, 18
Astropy Collaboration, Robitaille, T. P., Tollerud, E. J., et al. 2013, A&A, 558, A33
Becker, R. H., White, R. L., & Helfand, D. J. 1995, ApJ, 450, 559
Bizenberger, P., McCaughrean, M. J., Birk, C., Thompson, D., & Storz, C. 1998, in Society of Photo-Optical Instrumentation Engineers (SPIE) Conference Series, Vol. 3354, Society of Photo-Optical Instrumentation Engineers (SPIE) Conference Series, ed. A. M. Fowler, 825–832
Blain, A. W., Assef, R., Stern, D., et al. 2013, ApJ, 778, 113
Buzzoni, B., Delabre, B., Dekker, H., et al. 1984, The Messenger, 38, 9
Carilli, C. L., Neri, R., Wang, R., et al. 2007, ApJ, 666, L9
Condon, J. J., Cotton, W. D., Greisen, E. W., et al. 1998, AJ, 115, 1693
Cool, R. J., Kochanek, C. S., Eisenstein, D. J., et al. 2006, AJ, 132, 823
Cutri, R. M., e. 2012, VizieR Online Data Catalog, 2311, 0
De Rosa, G., Decarli, R., Walter, F., et al. 2011, ApJ, 739, 56
De Rosa, G., Venemans, B. P., Decarli, R., et al. 2013, ArXiv e-prints, arXiv:1311.3260
Decarli, R., Falomo, R., Treves, A., et al. 2010, MNRAS, 402, 2441
Diamond-Stanic, A. M., Fan, X., Brandt, W. N., et al. 2009, ApJ, 699, 782
Dupuy, T. J., & Liu, M. C. 2012, ApJS, 201, 19
Fan, X., Carilli, C. L., & Keating, B. 2006a, ARA&A, 44, 415
Fan, X., Narayanan, V. K., Lupton, R. H., et al. 2001, AJ, 122, 2833
Fan, X., Strauss, M. A., Schneider, D. P., et al. 2003, AJ, 125, 1649
Fan, X., Hennawi, J. F., Richards, G. T., et al. 2004, AJ, 128, 515
Fan, X., Strauss, M. A., Richards, G. T., et al. 2006b, AJ, 131, 1203
Fan, X., Strauss, M. A., Becker, R. H., et al. 2006c, AJ, 132, 117
Francis, P. J., Hewett, P. C., Foltz, C. B., et al. 1991, ApJ, 373, 465
Goto, T. 2006, MNRAS, 371, 769
Greiner, J., Bornemann, W., Clemens, C., et al. 2008, PASP, 120, 405
Güsten, R., Nyman, L. Å., Schilke, P., et al. 2006, A&A, 454, L13
Hamuy, M., Suntzeff, N. B., Heathcote, S. R., et al. 1994, PASP, 106, 566
Hamuy, M., Walker, A. R., Suntzeff, N. B., et al. 1992, PASP, 104, 533

Hinshaw, G., Larson, D., Komatsu, E., et al. 2013, ApJS, 208, 19
Hryniewicz, K., Czerny, B., Nikołajuk, M., & Kuraszkiewicz, J. 2010, MNRAS, 404, 2028
Hunter, J. D. 2007, Computing in Science and Engineering, 9, 90
Jiang, L., Fan, X., Annis, J., et al. 2008, AJ, 135, 1057
Jiang, L., Fan, X., Bian, F., et al. 2009, AJ, 138, 305
Kaiser, N., Aussel, H., Burke, B. E., et al. 2002, in Society of Photo-Optical Instrumentation Engineers (SPIE) Conference Series, Vol. 4836, Society of Photo-Optical Instrumentation Engineers (SPIE) Conference Series, ed. J. A. Tyson & S. Wolff, 154–164
Kaiser, N., Burgett, W., Chambers, K., et al. 2010, in Society of Photo-Optical Instrumentation Engineers (SPIE) Conference Series, Vol. 7733, Society of Photo-Optical Instrumentation Engineers (SPIE) Conference Series
Kurk, J. D., Walter, F., Fan, X., et al. 2007, ApJ, 669, 32
Lane, R. A., Shemmer, O., Diamond-Stanic, A. M., et al. 2011, ApJ, 743, 163
Laor, A., & Davis, S. W. 2011, MNRAS, 417, 681
Lawrence, A., Warren, S. J., Almaini, O., et al. 2007, MNRAS, 379, 1599
Magnier, E. 2006, in Proc. The Advanced Maui Optical and Space Surveillance Technologies Conf., ed. S. Ryan (Kihei: Maui Economic Development Board), E50
Magnier, E. 2007, in Astronomical Society of the Pacific Conference Series, Vol. 364, The Future of Photometric, Spectrophotometric and Polarimetric Standardization, ed. C. Sterken, 153
Mahabal, A., Stern, D., Bogosavljević, M., Djorgovski, S. G., & Thompson, D. 2005, ApJ, 634, L9
McGreer, I. D., Becker, R. H., Helfand, D. J., & White, R. L. 2006, ApJ, 652, 157
Meiksin, A. 2006, MNRAS, 365, 807
Metcalfe, N., Farrow, D. J., Cole, S., et al. 2013, MNRAS, 435, 1825
Meusinger, H., Schalldach, P., Scholz, R.-D., et al. 2012, A&A, 541, A77
Morganson, E., De Rosa, G., Decarli, R., et al. 2012, AJ, 143, 142
Mortlock, D. J., Patel, M., Warren, S. J., et al. 2012, MNRAS, 419, 390 Venemans, B. P., Findlay, J. R., Sutherland, W. J., et al. 2013, ApJ, 779, 24
—. 2009, A&A, 505, 97
Mortlock, D. J., Warren, S. J., Venemans, B. P., et al. 2011, Nature, 474, 616
Oke, J. B. 1990, AJ, 99, 1621
Pogge, R. W., Atwood, B., Brewer, D. F., et al. 2010, in Society of Photo-Optical Instrumentation Engineers (SPIE) Conference Series, Vol. 7735, Society of Photo-Optical Instrumentation Engineers (SPIE) Conference Series
Richards, G. T., Vanden Berk, D. E., Reichard, T. A., et al. 2002, AJ, 124, 1
Schuller, F. 2012, in Society of Photo-Optical Instrumentation Engineers (SPIE) Conference Series, Vol. 8452, Society of Photo-Optical Instrumentation Engineers (SPIE) Conference Series
Shemmer, O., Trakhtenbrot, B., Anderson, S. F., et al. 2010, ApJ, 722, L152
Shen, Y., Strauss, M. A., Oguri, M., et al. 2007, AJ, 133, 2222
Simcoe, R. A., Burgasser, A. J., Bernstein, R. A., et al. 2008, in Society of Photo-Optical Instrumentation Engineers (SPIE) Conference Series, Vol. 7014, Society of Photo-Optical Instrumentation Engineers (SPIE) Conference Series
Simcoe, R. A., Burgasser, A. J., Schechter, P. L., et al. 2013, PASP, 125, 270
Siringo, G., Kreysa, E., Kovács, A., et al. 2009, A&A, 497, 945
Skrutskie, M. F., Cutri, R. M., Stiening, R., et al. 2006, AJ, 131, 1163
Stubbs, C. W., Doherty, P., Cramer, C., et al. 2010, ApJS, 191, 376
Taylor, M. B. 2005, in Astronomical Society of the Pacific Conference Series, Vol. 347, Astronomical Data Analysis Software and Systems XIV, ed. P. Shopbell, M. Britton, & R. Ebert, 29
Taylor, M. B. 2006, in Astronomical Society of the Pacific Conference Series, Vol. 351, Astronomical Data Analysis Software and Systems XV, ed. C. Gabriel, C. Arviset, D. Ponz, & S. Enrique, 666
Tonry, J. L., Stubbs, C. W., Lykke, K. R., et al. 2012, ApJ, 750, 99
Vanden Berk, D. E., Richards, G. T., Bauer, A., et al. 2001, AJ, 122, 549
Venemans, B. P., McMahon, R. G., Warren, S. J., et al. 2007, MNRAS, 376, L76
Venemans, B. P., Findlay, J. R., Sutherland, W. J., et al. 2013, ApJ, 779, 24
Wang, R., Carilli, C. L., Wagg, J., et al. 2008, ApJ, 687, 848
Wang, R., Wagg, J., Carilli, C. L., et al. 2013, ApJ, 773, 44
Willott, C. J., Delfosse, X., Forveille, T., Delorme, P., & Gwyn, S. D. J. 2005, ApJ, 633, 630
Willott, C. J., McLure, R. J., & Jarvis, M. J. 2003, ApJ, 587, L15
Willott, C. J., Delorme, P., Omont, A., et al. 2007, AJ, 134, 2435
Willott, C. J., Delorme, P., Reylé, C., et al. 2009, AJ, 137, 3541
Willott, C. J., Albert, L., Arzoumanian, D., et al. 2010a, AJ, 140, 546
Willott, C. J., Delorme, P., Reylé, C., et al. 2010b, AJ, 139, 906
Wright, E. L., Eisenhardt, P. R. M., Mainzer, A. K., et al. 2010, AJ, 140, 1868
Zeimann, G. R., White, R. L., Becker, R. H., et al. 2011, ApJ, 736, 57